Inage and Projection Noise Transfer Analysis of Base Material Decomposed Spectral CT Data

Björn J. Heismann*[a,b]
a Siemens Medical Solutions, Computed Tomography Division
b Institute of Pattern Recognition, Friedrich-Alexander-University Erlangen-Nuremberg.

ABSTRACT

Image noise is a decisive issue for medical spectral CT applications. The Base Material Decomposition (BMD) as the standard spectral CT algorithm converts dual-energy scan data to material coefficient images. In this process the Poisson noise of the original CT measurement data is converted to noise in the coefficient images. A generalized method to evaluate this process has been developed. It gives us the factor by which the BMD algorithm increases both the projection and image noise of the material coefficient data. As a figure of merit we determine the noise amplification factors A_1, A_2. They are given by the ratio of the relative noise of the dual-energy projections B_1, B_2 to the relative noise of the combined projection data P. We apply the method to a typical dual-energy CT scan with 80kV and 140kV tube settings. For generic sets $\{P_1, P_2\}$ of dual-energy projections with $P_i = 10^{-4.5} \ldots 1$, both the water and bone decomposition and the Compton and Photoelectric Effect decomposition are analyzed. We find that for both the empirical (water and bone) and physical (Compton and Photoelectric Effect) decomposition the noise is generally amplified. The bone and Photo-Effect coefficients exhibit a noise increase of their respective coefficients by a factor of at least 2. For the main part of the projection P_1, P_2 plane it is in the range of 3 to 5. For small contributions of one base material, the noise amplification becomes critically large. In this case the water and bone base material decomposition is limited in use for quantitative CT since one of its coefficients is not usable for material identification. For the Compton and Photoelectric Effect decomposition physically both coefficients reach zero simultaneously and avoid the critical noise increase. For a partial region of the P_1, P_2 plane the Compton coefficient shows better noise performance than the combined raw data P. In conclusion the noise transfer properties of the physical decomposition are found to be superior to the empirical bone and water decomposition, both in terms of minimum image noise and usability for quantitative CT.

Keywords: Base Material Decomposition, noise transfer analysis, Computed Tomography

1. INTRODUCTION

Spectral CT aims at obtaining new object information from spectrally resolved CT measurements. The base material decomposition presented by Alvarez and Macovski in 1976 [1, 2] is mostly used for this purpose. It converts dual-energy CT measurements into two material coefficient images. Originally Compton and Photoelectric Effect attenuation formulae were used as base functions. These components physically add up to the spectral attenuation coefficient and thereby form a natural base system. The resulting coefficient data was used to characterize a number of clinically relevant tissue types by pairs of coefficients, see e.g. [3]. In the following empirical base functions like water and bone mineral attenuation functions were also implemented and optimized [4-7]. They have the advantage to provide intuitive decompositions of CT objects, like e.g. bone and soft-tissue images.
In the diagnostic use of the image data the noise introduced by the decomposition process is a decisive issue. Mathematically

the dual-energy projections P_1, P_2 are converted to coefficient projections B_1, B_2 which generally show increased relative noise. This not only obviously reduces the contrast-to-noise of the coefficient images. It also limits the promising quantitative use of pairs of coefficients for material characterization as proposed already in the original papers.
In this paper a generic method to analyze the noise transfer properties of dual-energy methods is described. Compared to earlier work [1-2] it quantifies the image and projection noise of BMD data without predetermining specific configurations of attenuators. It also fully takes into account the non-linear inversion process and a realistic description of the system energy weighting in the dual-energy detection process. We use it to investigate the noise transfer properties of the two most common decompositions, a) the water and bone and b) the Compton and Photoelectric Effect decomposition for a [80 kV, 140 kV] dual-energy scan.

2. THEORY

We first review the spectral CT formulae and energy weighting to develop the noise transfer properties of the Base Material Decomposition (BMD). The projection P in a CT measurement is given by

$$P = \frac{I}{I_0} = \int_E w(E) e^{-\int_{\{L\}} \kappa(E,\vec{r}) d\vec{r}} dE \tag{1}$$

with I := measured intensity with absorber, I_0 := measured intensity without absorber, $\kappa(E, \boldsymbol{r})$:= spectral attenuation coefficient, $\{L\}$:= X-ray path between source and detector. The weighting function $w(E)$ is

$$w(E) = \frac{S(E)D(E)}{\int_E S(E)D(E)dE} \tag{2}$$

with $S(E)$:= X-ray tube emission spectrum and $D(E)$:= detector spectral responsivity. $S(E)$ is given in quanta per energy and can be measured directly or modeled according to Boone's parameterization [9]. $D(E)$ describes the signal contribution for a quantum of energy E. For a standard integrating X-ray detector it corresponds to the average detected energy. In order to calculate it the physics of X-ray detection including fluorescence and Compton escapes and the information transport in the absorber have to be incorporated, see [8]. Fig 1 shows the weighting functions $w_1(E)$, $w_2(E)$ of typical 80 kV and 140 kV dual-energy measurements.

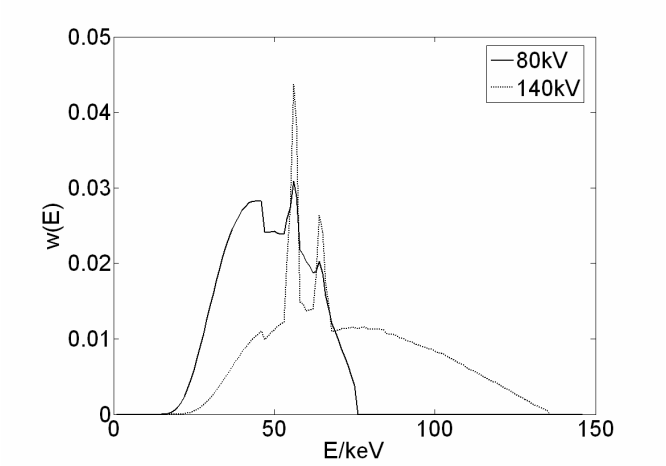

Fig 1. Dual-energy weighting functions w_1 and w_2 for 80 and 140 kV X-ray tube voltage measurements with a GdOS solid state CT detector.

Dual-energy measurements generate two sets of projections P_1, P_2 with different spectral weightings w_1, w_2:

$$\begin{pmatrix} P_1 \\ P_2 \end{pmatrix} = \begin{pmatrix} \int_E w_1(E) e^{-\int_{\{L\}} \kappa(E,\vec{r}) d\vec{r}} dE \\ \int_E w_2(E) e^{-\int_{\{L\}} \kappa(E,\vec{r}) d\vec{r}} dE \end{pmatrix}. \tag{3}$$

The base material decomposition method [1, 2] separates κ into spatial and spectral coordinates:

$$\kappa(E,\vec{r}) = b_1(\vec{r}) F_1(E) + b_2(\vec{r}) F_2(E) \tag{4}$$

$F_1(E)$, $F_2(E)$ are energy-dependent attenuation functions. We have basically two choices: Either we use 'Physical Modeling' with the Photoelectric Effect absorption and Compton scatter Klein-Nishina attenuation functions, as originally proposed by Alvarez and Macovski, or we employ 'Empirical Modeling' with effective base materials like water and bone mineral. In both cases the spatially-dependant coefficients b_1, b_2 describe the effective concentration of the two base materials. We can insert (4) into (3) to obtain a two-step process:

1. The measured projections P_1, P_2 are converted to B_1, B_2 by solving

$$\begin{pmatrix} P_1 \\ P_2 \end{pmatrix} = \begin{pmatrix} \int_E w_1(E) \left(e^{-F_1(E)}\right)^{B_1} \left(e^{-F_2(E)}\right)^{B_2} dE \\ \int_E w_2(E) \left(e^{-F_1(E)}\right)^{B_1} \left(e^{-F_2(E)}\right)^{B_2} dE \end{pmatrix}. \tag{5}$$

2. The B_1, B_2 are transformed to $b_1(\mathbf{r})$, $b_2(\mathbf{r})$ by solving

$$B_j = \int_L b_j(\vec{r})d\vec{r}, j = 1,2. \tag{6}$$

Eq. 5 and 6 fully describe the BMD data flow: Measured dual-energy sinograms P_1, $P_2 \rightarrow$ coefficient projections B_1, $B_2 \rightarrow$ coefficient images b_1, b_2.

Table 1

Variable	Variance	Remark
Measured quanta N_1 ,N_2	N_i	Poisson distributed, Can be modeled as Gaussian distr. for CT flux (N>~30)
Max. measured quanta $N_{0,1}$, $N_{0,2}$	*see remark*	Practically minimized by massive averaging during 'air-calibration' in CT
Dual-energy projections P_1, P_2	$P_i / N_{0,i}$	Measured projection $P_i = N_i / N_{0,i}$
Variable	Relative Noise	Remark
Combined projection (Eq. 8) P	*see Eq. 9*	Dual-energy measurements combined to standard single energy data
Coefficient projections B_1, B_2	*see Eq. 10*	Generally not Poisson / Gaussian distributed

Our target is to understand the noise transfer through this process. Usually, this is investigated [wiederholung, s.o.] by measuring or simulating specific object configurations and determining the SNR or CNR of selected partial image regions.

The linearity of the second step (Eq. 6) allows for a more general approach. Consider a set of projections i.e. a sinogram $\{B_j\}$ and an image volume $\{b_j\}$ reconstructed from it. If we increase the relative noise of all projections in $\{B_j\}$ by a factor of α, we also increase the relative noise of the image volume $\{b_j\}$ by the same factor α. The relative noise of a projection B_j is at the same time a measure for the relative noise in the image. Therefore the noise amplification

$$A_j \equiv \sigma_{rel}(B_j) / \sigma_{rel}(P), j = 1,2 \tag{7}$$

is defined to characterize the noise transfer of the BMD. It relates the relative noise of the coefficient projections B_j to the relative noise of the combined input projection

$$P = \frac{N_1 + N_2}{N_{0,1} + N_{0,2}} \tag{8}$$

Here N_1, N_2 is the measured number of quanta with attenuator and $N_{0,1}$, $N_{0,2}$ the maximum number of quanta measured without attenuator. Table 1 gives an overview of the notation used. The combined projection P fuses the two individual dual-energy projections to one projection set. This can be used for a standard CT reconstruction with the maximum number of quanta from both measurements. The relative noise of P for uncorrelated dual-energy measurements with dual-kVp settings is

$$\sigma_{\mathrm{rel}}(\mathrm{P}) = \frac{1}{\sqrt{\mathrm{P}_1 N_{0,1} + P_2 N_{0,2}}}. \tag{9}$$

since the contribution of $\sigma(N_{0,i})$ can be neglected in CT due to averaging.

In order to calculate

$$\sigma_{rel}(B_j) = \sqrt{\mathrm{var}(B_j)} \Big/ B_j \tag{10}$$

we first convert (P_1,P_2) to $(B_1(P_1,P_2), B_2(P_1,P_2))$ according to Eq. 5. Secondly we calculate the mean

$$\langle B_j \rangle = \int\int g(P_1, P_2) B_j(P_1, P_2) dP_1 dP_2 \tag{11}$$

and variance

$$\mathrm{var}(B_j) = \int\int g(P_1, P_2) \left(\langle B_j \rangle - B_j(P_1, P_2) \right)^2 dP_1 dP_2 \tag{12}$$

from the $B_1(P_1,P_2)$, $B_2(P_1,P_2)$ functions. Here, the normalized 2D Gaussian weighting function

$$g(P_1, P_2) = \frac{1}{2\pi\sigma(P_1)\sigma(P_2)} \exp\left(-\frac{(\langle P_1 \rangle - P_1)^2}{2\sigma^2(P_1)} \right) \exp\left(-\frac{(\langle P_2 \rangle - P_2)^2}{2\sigma^2(P_2)} \right) \tag{13}$$

describes the probability density to measure a set of projections P_1, P_2 for given means $\langle P_1 \rangle$, $\langle P_2 \rangle$ and standard deviations $\sigma(P_1)$, $\sigma(P_2)$[1].

Eq. 11-13 simulate the measurement process. The distribution of the input projections P_1, P_2 is transferred to statistics of B_1, B_2. We insert the results of Eq. 11 and 12 into Eq. 10 and obtain the noise amplifications A_j of Eq. 7. As our figures of merit they yield the factor by which the noise of the coefficient projections and images exceeds the noise of the standard CT input data.

[1] It should be noted that this model set-up does not include noise correlations and electronic noise in the input data. Both can be implemented directly by using adjusted $\sigma_{rel}(P_1)$, $\sigma_{rel}(P_2)$,$\sigma_{rel}(P)$ and an adequate correlated weighting function $g(P_1, P_2)$.

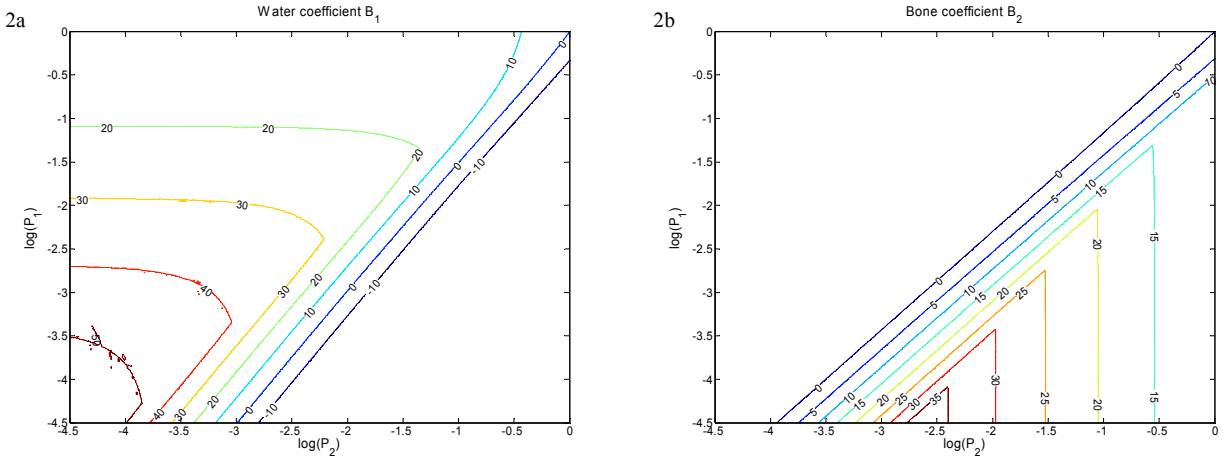

Figs 2a, 2b: Base material decomposition into water (2a) and bone (2b) component.

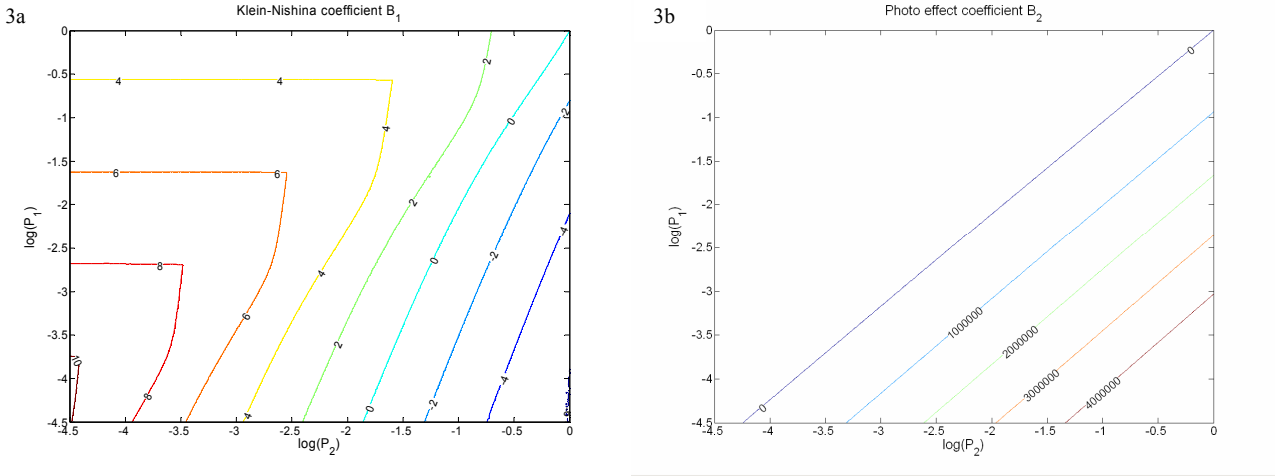

Figs 3a, 2b: Base material decomposition into Compton Effect (3a) and Photoelectric Effect (3b) component.

3. RESULTS AND DISCUSSION

We assume a typical dual-energy CT measurement with the w_1, w_2 of Fig. 1 and maximum quantum numbers of $N_{0,1} = N_{0,2} = 2.5 \cdot 10^5$. For inverting Eq. 5 a non-linear numerical fit with a relative error margin $\delta < 1e^{-6}$ yields the $B_j(P_1,P_2)$, $j = 1,2$. A grid $P_i = [10^{-4.5}, 1]$, $i = 1, 2$ with spacing $\Delta\log(P_i) = 0.01$ is used. Figures 2a, 2b show the B_1, B_2 for the bone and water decomposition and Figures 3a, 3b show B_1, B_2 for the Compton and Photoelectric Effect decomposition. Note that the bone and water coefficient projections can reach zero individually. This is not the case for the physical decomposition into Compton and Photoelectric Effect coefficients. They only reach zero simultaneously, corresponding to $\mu = 0$, since they are both approximately linear in the density of the absorber.

The noise amplifications A_1, A_2 have been calculated according to Eq. 7. They are shown in Figures 4a, 4b for the water and bone decomposition and Figures 5a, 5b for the Compton and Photoelectric Effect decomposition. The thick lines surround the area where both B_1 and B_2 are positive. For the water and bone decomposition negative coefficient values are possible for non-base materials, see e.g. [7, 11]. For the Compton and Photoelectric Effect decomposition the thick lines surround the physically valid part of the P_1, P_2 plane. Only noise and scattering portions in the projection data create negative coefficient values.

We first analyze the water and bone decomposition results of Figures 4a, 4b: For both A_1 and A_2 the noise is significantly amplified in most of the valid area. The water coefficient noise amplification A_1 is > 1 for almost all values of the positive coefficient region. The bone coefficient noise amplification A_2 is > 2 respectively. Note that the noise amplification increases critically for both B_i when they approach small values. Since both coefficients can be zero individually this property is an issue for the water and bone decomposition. Consider e.g. the decomposition of soft body tissue. Since it is mainly composed of water, the bone coefficient will be $B_2 \approx 0$. It will not be possible to use the resulting coefficient pair as a precise identifier for tissue characterization.

The Compton and Photoelectric Effect decomposition (Figures 3 and 5) show the larger positive region of the coefficients B_1 and B_2 marked by thick lines. The Compton coefficient shows a noise decrease $A_1 < 1$ for a part of this region. This is due to the fact that the $\exp(-F_{Klein\_Nishina}(E))$ function is nearly a constant function offset which can be recovered with superior precision. In practical CT this potential benefit is probably reduced by the decreased contrast of the Compton image.
The Photoelectric Effect noise amplification A_2 is >2 for most of the positive coefficient region. Since the B_1 and B_2 can only be zero simultaneously the critical noise increase is not present here.

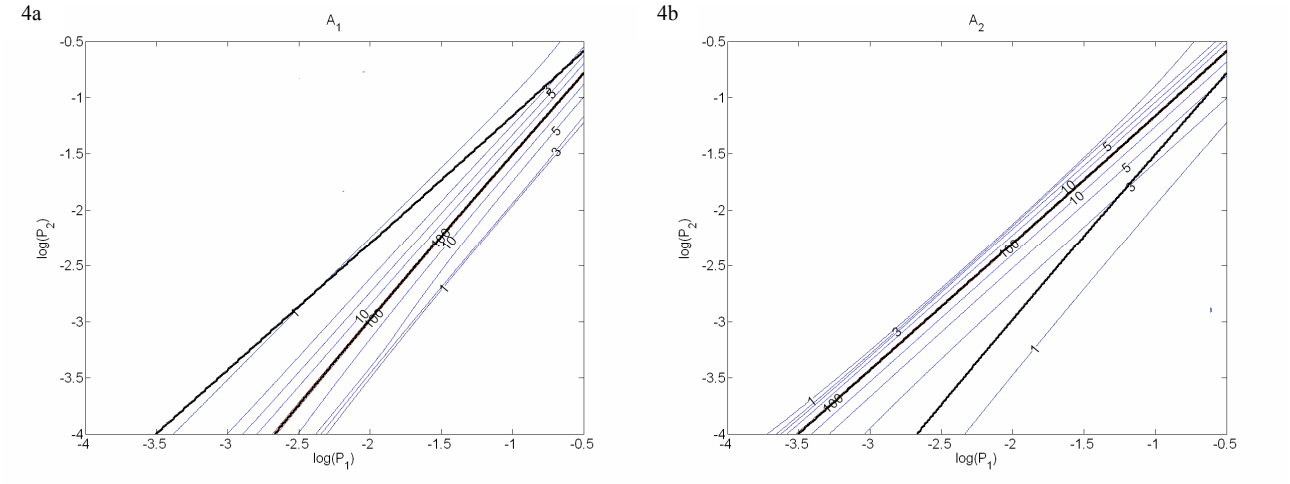

Figs. 4a, 4b: Noise increase of the water and bone decomposition for the bone (4a) and water (4b) coefficient. The thick lines mark the region where both coefficients in Figs. 2a, 2b are positive.

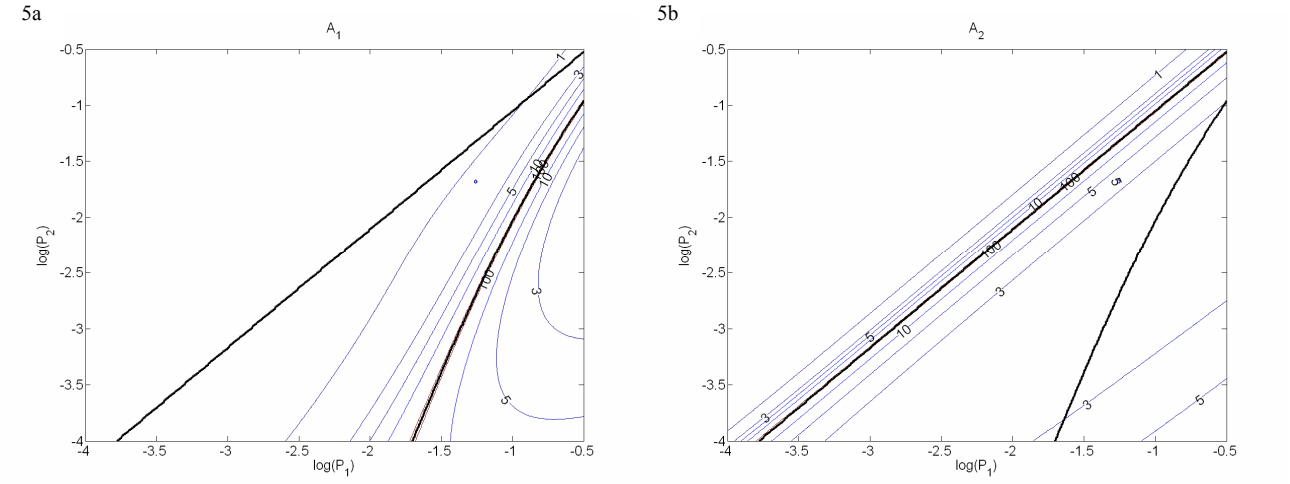

Figs. 5a, 5b: Noise increase of the Klein-Nishina (5a) and Photoelectric Effect component (5b). The thick lines mark the region where both coefficients in Figures.3a, 3b are positive. Note that the positive region is large than in Figures. 4a, 4b.

4. SUMMARY

A noise transfer system model for base material decomposition algorithms has been developed. The noise amplification as the ratio of the relative noise of the coefficient projection to the relative noise of the combined input data is defined and evaluated as a figure of merit. It is applied to the case of a typical dual-energy [80 kV, 140 kV] spectral CT acquisition with uncorrelated Poisson noise and both physical and empirical base function systems. For the empirical base system we find minimum noise amplifications $A_{Water} > 1$ and $A_{Bone} > 2$. Both noise amplifications rise strongly with the corresponding coefficients approaching zero. This has significant impact on the quantitative usage of decomposition methods with empirical modeling. Both soft tissue and bone material projections yield a corresponding coefficient close to zero. Its noise amplification is large. This reduces the characterization accuracy of tissue or materials by a pair of coefficients significantly. For the physical base system the coefficients and their projections are both approximately linear in the attenuator density. They reach zero only for $\mu = 0$, so there is no critical noise amplification here. The minimum noise amplification of the Photoelectric coefficient projections and images is found to be $A_{Photo} > 2$. The Compton coefficient shows a noise decrease $A_{Compton} < 1$ for parts of the P_1, P_2 plane. This is due to the fact that the Klein-Nishina exponential $\exp(-F_{KleinNishina}(E))$ is nearly a constant function. The corresponding coefficient can be recovered with greater precision. Further work will compare these generic findings to specific object configurations, including an analysis of the contrast-to-noise behavior of Compton coefficient images.

In conclusion the noise transfer behavior of the physical decomposition is superior in two respects to the empirical decomposition: The noise is globally less amplified by the decomposition process and a quantitative characterization of body tissue is conceivable for arbitrary materials. Still, the analysis shows that the decomposition process increases especially the noise for the high attenuating function coefficient significantly. This has to be justified by the potential diagnostic value of the coefficient image contrasts and quantitative characterization values.

5. BIBLIOGRAPHY

1. R.E. Alvarez. A. Macovski, Phys. Med Biol. 21(5):733-44 (1976)
2. A. Macovski, R.E. Alvarez. J.L. Chan. J.P. Stonestrom. L.M. Zatz, Comp. Biol. Med. 6(4):325-36 (1976)
3. M.E. Phelps. E.J.Hoffman and M.M. Ter-Pogossian, Radiology, 117, 573 (1975)
4. J.B. Weaver, A.L. Huddleston, Med. Phys. 12(1) 40-45 (1985)
5. J.P. Stonestrom, R.E. Alvarez, A. Macovski, IEEE Trans. Biomed. Eng. Vol. BME-28, No. 2 , 128(1981)
6. J.R. Vetter and J.E. Holden, Med. Phys. 15(5), 728 (1988)
7. W.A. Kalender, W.H. Perman, J.R. Vetter, E. Klotz, Med Phys 13, 334-339 (1986)
8. S. Wirth, K. Pham-Gia, W.Metzger, B.J. Heismann, M11-212, IEEE Medical Imaging Conference Record (2006)
9. J.M. Boone, J.A. Seibert, Med. Phys. 24, 1661-1670 (1997)
10. B.J. Heismann, M11-366, IEEE Medical Imaging Conference Record (2005)